### Title

Beneficial Effects of Cerium Oxide Nanoparticles in Development of Chondrocyte-Seeded Hydrogel Constructs and Cellular Response to Interleukin Insults




### Journal

Tissue Engineering Part A, 20(21-22)

### ISSN

1937-3341



### Authors

Ponnurangam, Sathish
O'Connell, Grace D
Chernyshova, Irina V
et al.



### Publication Date

2014-11-01

### DOI

10.1089/ten.tea.2013.0592

Peer reviewed

TISSUE ENGINEERING: Part A
Volume 20, Numbers 21 and 22, 2014

DOI: 10.1089/ten.tea.2013.0592

# Beneficial Effects of Cerium Oxide Nanoparticles in Development of Chondrocyte-Seeded Hydrogel Constructs and Cellular Response to Interleukin Insults

Sathish Ponnurangam, PhD,[1] Grace D. O'Connell, PhD,[2] Irina V. Chernyshova, PhD,[1] Katherine Wood, MS,[3] Clark Tung-Hui Hung, PhD,[3] and Ponisseril Somasundaran, PhD[1]

The harsh inflammatory environment associated with injured and arthritic joints represents a major challenge to articular cartilage repair. In this study, we report the effect of cerium oxide nanoparticles, or nanoceria, in modulating development of engineered cartilage and in combating the deleterious effects of interleukin-1α. Nanoceria was found to be biocompatible with bovine chondrocytes up to a concentration of 1000 μg/mL (60,000 cells/μg of nanoceria), and its presence significantly improved compressive mechanical properties and biochemical composition (i.e., glycosaminoglycans) of engineered cartilage. Raman microspectroscopy revealed that individual chondrocytes with internalized nanoceria have increased concentrations of proline, procollagen, and glycogen as compared with cells without the nanoparticles in their vicinity. The inflammatory response due to physiologically relevant quantities of interluekin-1α (0.5 ng/mL) is partially inhibited by nanoceria. To the best of the authors' knowledge, these results are the first to demonstrate a high potential for nanoceria to improve articular cartilage tissue properties and for their long-term treatment against an inflammatory reaction.

## Introduction

Osteoarthritis and cartilage injuries are a major cause of disability. Cell-based therapies, including tissue engineering, are being explored as a potential repair strategy. Inflammatory response or graft rejections by the host are among the major challenges for any implanted material.[1–4] In cartilage tissue engineering, several strategies have been tested to overcome these problems. For instance, it has been shown that cultivating partially or fully mature engineered cartilage *in vitro* allows implanted tissue to withstand the harsh catabolic environment better than a freshly seeded or underdeveloped construct.[5,6] Other strategies include delivery of steroids, such as dexamethasone, or exogenous cross-linking factors.[6–8] However, biocompatible substances that sustainably scavenge radicals and protect *de novo* cartilage from an inflammatory response are more advantageous. In this study, we investigated the effect of cerum oxide nanoparticles in culture to act as a protectant for engineered cartilage against cytokine exposure.

Cerium oxide nanoparticles (nanoceria) can potentially play an anti-inflammatory role for engineered cartilage because of its capacity to scavenge reactive oxygen and nitrogen species, combat inflammation, downregulate cytokine levels, and confer cell protection both *in vitro* and *in vivo*.[9] Importantly, nanoceria has been shown to prevent accumulation of nitrosative stress biomarkers,[10,11] such as nitrated proteins, which are a leading cause for graft rejection.[12,13] Previous studies demonstrated that nanoceria protects several mammalian cell types, including neural,[14,15] retinal,[16] hepatic,[17] cardiac,[10] breast,[18] and epidermal cells, from oxidative stresses and inflammatory responses.[19] Interestingly, nanoceria decreases tumor cell viability and invasive capacity, while being nontoxic to normal cells.[20–23] Nanoceria has been found to have deleterious effects on human bronchoalveolar cancer cells through generation of free radicals and membrane damage, which decreased the cellular viability.[24] On the contrary, several reports suggest pro-oxidant cytotoxic effects of nanoceria under both *in vivo* and *in vitro* conditions.[25–29] The recent work presented in the literature suggests that the synthesis, processing, storage, and handling of nanoceria can have a significant impact on the pro-oxidative and antioxidative properties, and that a comprehensive physicochemical characterization of the nanoparticles is needed.[30] However, nanoceria has not been investigated for either pro-oxidant or antioxidant effects on chondrocytes.

There is a consensus that the radical-scavenging properties of nanoceria are based on reversibility of the $Ce^{3+}/Ce^{4+}$

[1]Department of Earth and Environmental Engineering, Columbia University, New York, New York.
[2]Department of Mechanical Engineering, University of California, Berkeley, California.
[3]Department of Biomedical Engineering, Columbia University, New York, New York.

redox couple with the consequent formation/annihilation of surface defects (oxygen vacancies).[31,32] Specifically, a partially reduced cerium oxide has oxygen vacancies or defects in the lattice structure, which are associated with the loss of oxygen in the reaction [Eq. (1)]. However, the non-stoichiometric oxide $CeO_{2-\delta}$ is readily reoxidized back to $CeO_2$ by oxygen. The oxidized $CeO_2$ nanoparticles are readily reduced when placed in water[14] or coated by PEG.[33]

$$CeO_2 \leftrightarrow CeO_{2-\delta} + \delta/2O_2 \quad (1)$$

On the basis of previous studies with nanoceria, we hypothesize that the presence of nanoceria during *in vitro* culture of chondrocytes protects the elaborated extracellular matrix (ECM) from degradation by cytokines (e.g., interleukin-1α [IL-1α]) and improves ECM production. We selected the IL-1α isoform for our study, because it has been shown to inhibit engineered cartilage growth and to damage developed tissue.[6,8,34] To test these hypotheses, we cultured juvenile bovine chondrocytes in an agarose hydrogel scaffold with various concentrations of nanoceria and IL-1α. We measured their mechanical and biochemical properties at certain time intervals. We used Raman microspectroscopy to extract additional molecular-level information about the response of chondrocytes to nanoceria and to verify the macroscopic data.

## Materials and Methods

### *Materials*

$CeO_2$ nanoparticles were obtained from Meliorum Tech (batch No. 121008; Rochester, NY). Low-melting-point type VII agarose, collagen type II from chicken sternal cartilage, and solid sodium dodecanoate were acquired from Sigma-Aldrich (St. Louis, MO). High-glucose Dulbecco's modified Eagle's medium (DMEM) powder, and live/dead cellular viability assay were obtained from Life Technologies (Grand Island, NY).

### *Cell culture*

Articular cartilage was harvested from knee joints of juvenile bovine obtained from the local abattoir. Primary chondrocytes were isolated through enzymatic digestion using collagenase (Type IV; Worthington, Inc., Westville, NJ)[35] and expanded in 500-$cm^2$, tissue-culture-treated dishes with a plating density of 20,000 cells/$cm^2$. Cells were cultured in a 5% $CO_2$ environment at 37°C and fed with DMEM media supplemented with 10% fetal bovine serum, amino acids (0.5× minimum essential amino acids and 1× nonessential amino acids), 0.5 ng/mL basic fibroblast growth factor, 0.5 ng/mL platelet-derived growth factor, and 1 ng/mL of transforming growth factor (TGF)-$\beta_1$ (Invitrogen Co., Carlsbad, CA), and antibiotics (100 units/mL penicillin and 100 μg/mL streptomycin) every 2 days. Once confluence was reached, chondrocytes were trypsinized and casted into a 2% w/v agarose slab at cell concentration of $60 \times 10^6$ cells/mL. Samples were cored from the slab with dimensions of 4 mm in diameter and a thickness of 2.34 mm. Constructs were cultured in chemically defined medium (CM: DMEM with 0.1 μM dexamethasone, 40 mg/mL L-proline, 50 mg/mL ascorbate 2-phosphate, 100 mg/mL sodium pyruvate, 1×ITS+premix, 100 U/mL penicillin and 100 mg/mL streptomycin, and amphotericin B) supplemented with TGF-$\beta_3$.[6] TGF-$\beta_3$ supplementation was stopped after day 14, because previous studies reported improved mechanical and biochemical properties of engineered cartilage with transient application of the growth factor.[36] Constructs were cultured for 2–3 weeks to allow their partial maturation before applying the IL-1α insult.[6]

### *Experimental design*

Two separate studies were performed to evaluate the anti-inflammatory effect of nanoceria particles on engineered cartilage. Study 1 investigated the effect of nanoceria incorporated within the agarose scaffold, and Study 2 evaluated the effect of supplementing the CM with nanoceria.

In Study 1, nanoceria particles were incorporated in the agarose gel at concentrations 0, 10, 100, and 1000 μg/mL, with the 0 μg/mL group serving as the control (Fig. 1A). Since chondrocytes were encapsulated in the agarose at a concentration of $60 \times 10^6$ cells/mL, the highest nanoceria (1000 μg/mL) loading group corresponds to 60,000 cells/μg of nanoceria at day 0. Nanoceria was mixed with liquid agarose during casting. A concentration of 10 ng/mL of IL-1α was added fresh to the CM during media changes between days 16 and 30.

In Study 2, the CM was supplemented with nanoceria at concentrations of 0, 100, and 1000 μg/mL, with the 0 μg/mL group serving as the control (Fig. 1B). Constructs were cultured for 21 days to obtain mechanical strength suitable for the IL-1α insult. On day 21, constructs were divided into 9 (3 IL-1α concentrations × 3 nanoceria concentrations) experimental groups to evaluate the effect of IL-1α concentration and nanoceria concentrations. IL-1α was applied at concentrations of 0, 0.5, or 10 ng/mL, and nanoceria was added at concentrations of 0, 100, or 1000 μg/mL. The group with 0 ng/mL of IL-1α and 0 μg/mL of nanoceria served as

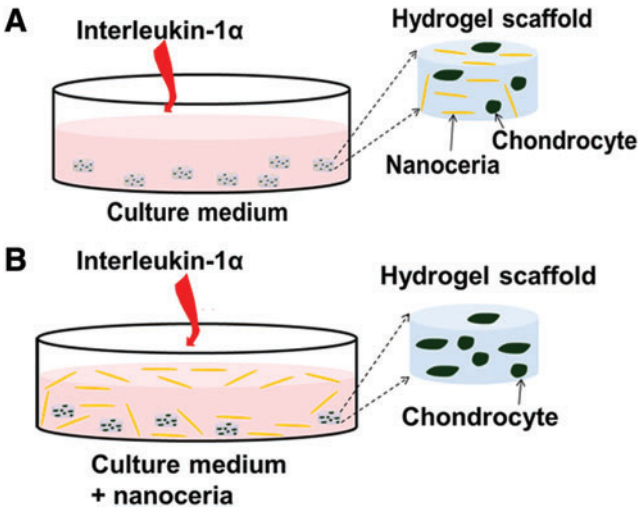


**FIG. 1.** Two modes of introducing nanoceria in a 3D agarose-based culture of chondrocytes. **(A)** In Study 1, nanoceria is embedded in the construct during casting (day 0) and interleukin-1α (IL-1α) is added to the culture media. **(B)** In Study 2, the growth medium is supplemented with nanoceria along with IL-1α. IL-1α was added fresh during each media change. 3D, three-dimensional. Color images available online at www.liebertpub.com/tea

the control. The intermediate IL-1α concentration of 0.5 ng/mL was selected to represent *in vivo* conditions,[37,38] whereas 10 ng/mL is known to be an effective concentration for inflammatory damage under *in vitro* conditions.[6,7,39,40]

Cell viability was evaluated using live/dead cytotoxicity kit (Life Technologies) and examined using a confocal microscope (Olympus Fluoview-100, Center Valley, PA). Living cells were stained with calcein-AM, which fluoresces green, and dead cells were stained with ethidium homodimer-1, which fluoresces red.

### *Mechanical properties*

Compressive mechanical properties of engineered cartilage were determined using a custom-made mechanical tester.[41] A stress-relaxation protocol was used in unconfined compression to determine the equilibrium Young's modulus, where 10% strain was applied at a strain rate of 0.05%/s, held for 30 min, and the equilibrium stress was used to calculate the modulus. The dynamic modulus was then measured by imposing 2% sinusoidal strain at a frequency of 1 Hz. Mechanical testing was performed every 2 weeks ($n = 4$–7 constructs per group).

### *Biochemical content*

Following mechanical testing, samples were weighed to obtain the wet weight and prepared for biochemistry. Constructs were dried by lyophilization for 48 h and digested using Proteinase K for 16 h at 56°C.[42] Agarose was centrifuged and the supernatant was collected to measure DNA, glycosaminoglycan (GAG), and collagen contents. The GAG content was measured spectrophotometrically using 1,9-dimethylmethylene blue (DMMB) dye-binding assay and compared to chondroitin-6-sulfate standards.[43,44] The collagen present in the digested sample was calculated by measuring ortho-hydroxyproline (OHP) content through a colorimetric procedure, and a collagen-to-OHP ratio of 7.64 was used to calculate the collagen content.[45] Biochemical contents (GAG, collagen, and DNA) were normalized by the construct's wet and dry weight.

### In vitro *confocal Raman microspectroscopy*

Nonpolarized Raman spectra were measured in two ranges of 300–1200 and 1180–1800 $cm^{-1}$ on individual living chondrocytes in ~1-mm-sliced sections of constructs immersed in CM. For the measurements, a LABRAM-ARAMIS confocal Raman microscope was used with a 17-mW, 633-nm HeNe laser as the excitation source. This excitation wavelength was found to be optimal for balancing between the Raman scattering efficiency and the detrimental interference from fluorescence. To reduce sample heating, the beam was attenuated by a D0.3 filter, and the power on the sample was 5.7 mW. To attain a satisfactory signal-to-noise ratio, spectra were acquired for 30 min each, using a 1200 grooves/mm diffraction grating and a UPlanApo/IR 60× (Olympus) water-immersion objective. The exposure of cells to the 633-nm irradiation with a power of 5.7 mW for 30 min was verified to be noninvasive since no change in the cell morphology was visually detected after the measurements. Moreover, the spectra measured during 3 min were qualitatively identical to the spectra measured during 30 min. The microscope wavenumber was calibrated before each set of measurements using the zero-order peak and the Si peak at 520.7 $cm^{-1}$ of a Si reference sample.

The pinhole size (350 μm) was selected to be optimal for probing a whole chondrocyte (with average size of 10 μm) with a minimum contribution from the ECM. Additional Raman measurements with a focus on the ECM regions, as well as Raman spectra of agarose hydrogel, confirmed that the spectra of the cells are qualitatively different from those of the scaffold matrix as the latter do not contain peaks of DNA and phospholipids. We did not use the ECM spectra for the analysis due to the statistically large deviations observed and much lower spectrum intensities. The standard deviation of the diagnostic bands was calculated separately and reported in the average spectra presented. The statistical analysis and the spectrum baseline correction procedure are demonstrated in Supplementary Figs. S5 and S6 (Supplementary Data are available online at www.liebertpub.com/tea) for the control sample. The Raman spectra of chondrocytes were processed using the Labspec software. Specifically, the spectra were uniformly smoothed using a Savitzky-Golay function (degree 4, size 13, and height 10). The baseline of the averaged spectra was corrected in the 400–1200- and 1200–1800-$cm^{-1}$ regions with a power-4 polynomial and a straight line, respectively (Supplementary Fig. S5).

Since the goal of the Raman study was to understand how individual chondrocyte cells interact with nanoceria, we acquired spectra of individual cells for 30 min each to attain a sufficient signal-to-noise ratio for each cell. This fact and the need to test all the samples within a couple of days limited our analysis to four to six cells per a sample. It should be mentioned that a more conventional approach (fast measurement of Raman spectra of 30–40 cells/sample and their statistical analysis) does not allow comparing cells that internalized nanoceria with those that did not. To verify whether the chosen reductionist approach is sensible, we repeated a part of these experiments both in the presence (1000 μg/mL) and absence of nanoceria but without IL-1α on more than 30 cells/sample. We have obtained similar trends between the mechanical strengths of the scaffolds and the spectra (in terms of intensities of the characteristic peaks) averaged over 30 and 5 cells (Supplementary Figs. S10 and S11).

### *Transmission electron microscopy*

Transmission electron microscopy (TEM) was used to evaluate average particle size and morphology of the cerium oxide nanoparticles (Jeol JEM 100CX, bright-field mode at 100 keV). The TEM samples were prepared by adding a drop of a dilute suspension of nanoceria onto a carbon-covered Cu, 300-mesh grid.

### *Statistical analysis*

A one-way ANOVA was performed on the Young's and dynamic moduli as well as biochemical content to test for differences between experimental groups. A *post hoc t*-test with two samples assuming equal variances was performed to obtain significant differences between individual groups with control. The significant difference across groups ($p$-value) and the number of samples ($n$) in a group are reported. The standard errors were calculated and were used for error bar values.

## Results

### *Characterization of nanoceria*

TEM images of nanoceria showed a rod-like morphology with an average aspect ratio of 8, where the particle dimensions were $65 \pm 10$ nm (length) and $8 \pm 1$ nm (width; Fig. 2). Polyhedral-shaped particles of 8-nm size were also noted; however, it cannot be fully ascertained whether the rounded nanoparticles are indeed a separate polyhedral particle or rod-like particles with a diameter of 8 nm oriented perpendicular to the microscope axis. As discussed in more detail in Supplementary Data, Raman spectra of the nanoceria show that even though the lattice structure of the nanoparticles is fluorite cubic, they contain a significant amount of the $Ce^{3+}$ lattice defects in the superficial layer. X-ray photoelectron spectroscopy (XPS) and UV-Vis absorption spectroscopy provide additional evidence of the relatively high concentration of $Ce^{3+}$ in the nanoparticles (Supplementary Figs. S3 and S4). In addition, XPS certifies that the nanoceria surface does not contain foreign elements. The surface area ($101 \pm 5\ m^2/g$) and isoelectric point ($\sim 7.5$) of the nanoparticles were measured using the Brunauer, Emmet, and Teller and electrokinetic methods, respectively (Supplementary Data).

### *Study 1*

Incorporation of nanoceria particles into the agarose scaffold at a concentration of 1000 μg/mL significantly improved mechanical properties of grown tissue in the absence of IL-1α (Fig. 3A, B). Direct contribution of nanoceria to the mechanical strength of the scaffold was ruled out because there were no significant differences across the groups at day 0 ($p > 0.6$, $n = 4$). The effect of 10 μg/mL nanoceria on the mechanical and biochemical properties was not significantly better than the control (Fig. 3). The biochemical analyses of these samples revealed an interesting pattern (Fig. 3C, D). DNA content was not significantly different across the various groups but the GAG content of the 1000 μg/mL nanoceria group was 15–20% greater than the control group ($p < 0.01$, $n = 4$). Thus, the nanoceria particles improved mechanical properties of engineered cartilage through increased biosynthesis of GAGs.

Nanoceria particles incorporated in the agarose scaffold did not prevent tissue degradation following insult with 10 ng/mL IL-1α (Fig. 3). Following IL-1α insult, the mechanical properties decreased to $40.8 \pm 2$ kPa ($n = 4$ per group) and were not significantly different from the control (Fig. 3). Biochemical analyses showed that GAG and collagen contents decreased with IL-1α (Fig. 3C, D). Cell viability on day 30 was similar across all groups (Fig. 4) and was confirmed by the DNA content (Fig. 3E).

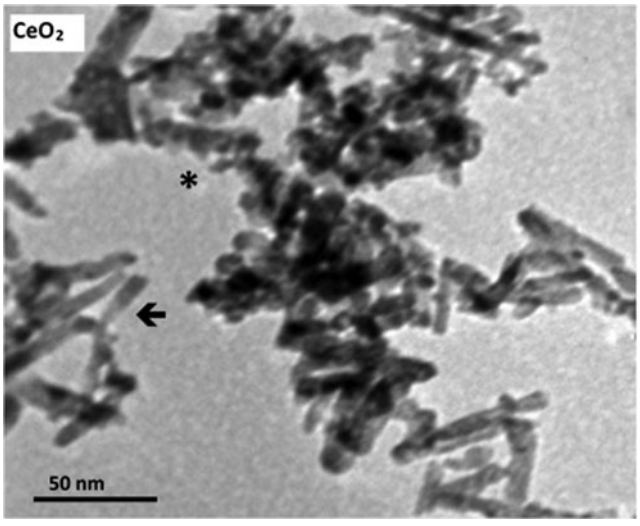


**FIG. 2.** Transmission electron microscopy image of nanoceria particles. Rod-shaped (arrows) and polyhedral (asterisks) particles.

Effects of nanoceria on chondrocytes and synthesis of proteins: *in vitro* Raman microspectroscopic analysis. To understand how individual chondrocyte cells interact with nanoceria, we performed a Raman microscopic study of individual chondrocyte cells in the scaffolds from Study 1. To be able to accurately differentiate between the Raman signatures of individual cells in the proximity of nanoceria from those of the cells remote from the nanoparticles, we limited out probing set to 5–10 cells/sample in order to attain a satisfactory signal-to-noise ratio in the individual spectra (see Experimental Design section for more detail).

Before presenting the results, it is worth noting that optical images of the cells subjected to the Raman analysis do not reveal significant changes in the cell morphology caused by the presence of 1000 μg/mL nanoceria (Fig. 5). To extract the molecular information from the Raman spectra, it is required to select diagnostic peaks for each biochemical component of the cell. For this purpose, we assigned spectral peaks by comparison of the Raman spectra of chondrocytes in scaffolds with those of chondrocytes in native cartilage, collagen type II from chicken sternal cartilage, agarose, and solid sodium dodecanoate (Supplementary Fig. S7), as well as with the literature spectra of phospholipids, glycogen, GAGs, DNA/RNA, and proteins.[46–48] This allowed us to distinguish for each cellular component several characteristic peaks that do not overlap with other peaks and have intensity much higher than the signal-to-noise ratio of the spectra of individual cells. These peaks and their analytical attributes are summarized in Table 1. Figure 6 compares the average Raman spectrum of cells in the control group ($n = 5$; constructs without nanoceria) with spectra of five individual cells from constructs that were embedded with 1000 μg/mL nanoceria. The five spectra of the nanoceria-exposed cells can be divided into two distinct groups. Spectra of cells 1, 4, and 6 are similar, within the standard deviation, to the average spectrum of the control sample. Moreover, these spectra do not display the $CeO_2$ peak at $460\ cm^{-1}$, suggesting that there is no detectable amount of nanoceria within the probing spot. In contrast, the spectra of cells 3 and 5 displayed a distinct nanoceria peak at $460\ cm^{-1}$ and are quantitatively different from the control. Further, they have significantly higher intensities of the Pro peak at $855\ cm^{-1}$, the glycogen peak at $480\ cm^{-1}$, and a peak at $940\ cm^{-1}$ due to the C−C stretching mode of α-helical structure of procollagen. The intensity for DNA at $\sim 790\ cm^{-1}$ was significantly different from the control group, which is in agreement with the biochemical properties reported previously. Optical images of the cells (Fig. 5) are

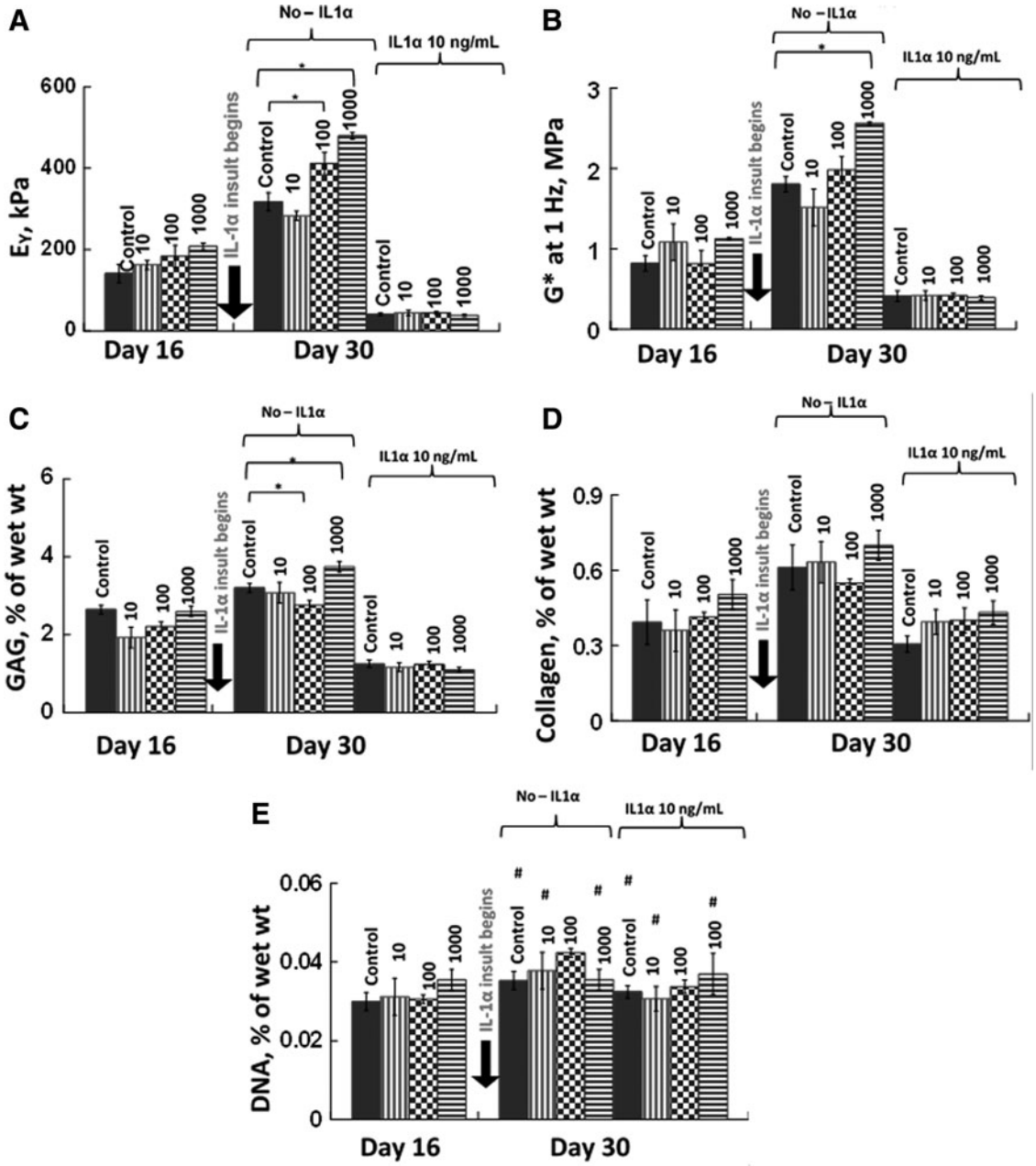


**FIG. 3.** Mechanical and biochemical properties for Study 1. Nanoceria particles were added to the agarose scaffold at concentrations of 0, 10, 100, and 1000 μg/mL. **(A)** Equilibrium Young's modulus ($E_Y$), **(B)** dynamic modulus ($G^*$) at 1 Hz, **(C)** glycosaminoglycan (GAG), and **(D)** collagen contents normalized by wet weight, and **(E)** DNA content ($n = 4$–7 per group per time point). * Represents $p < 0.05$. The DNA content did not vary significantly with addition of nanoceria or IL-1α ($^{\#}p > 0.1$). No significant difference in $E_Y$ and $G^*$ was observed across the groups on day 0 ($p > 0.6$).

consistent with the Raman-derived internalization of nanoceria, where cells contain large dark spots (Fig. 5C, D, arrow 1) with irregular shape as distinct from rounded and smaller lipid droplets. Moreover, Raman spectrum of a large dark spot inside the ECM (Fig. 5C, arrow 2) shows that this spot consists of nanoceria. In contrast, such large irregular spots are not observed inside cells 1 and 4 (Fig. 5A, B, respectively), as well as in images of control samples (Fig. 5E, F).

In addition, cells in contact with aggregates of nanoceria were characterized by lower peak intensities at 1300 and 1660 $cm^{-1}$, which represent common and unsaturated lipids, respectively (Table 1). Nanoceria was not observed to cause excessive lipid accumulation, even at high loading concentrations. This suggests that nanoceria does not trigger the apoptotic mechanism linked to excessive lipid accumulation.[49] This result agrees with the results from DNA content analysis and live/dead viability staining (Figs. 3E and 4). Finally, Raman analysis did not detect spectral markers of DNA damage, which would be noted as increased Raman peaks at 1578 $cm^{-1}$ and new peaks at 1607 or 1114 $cm^{-1}$, which correspond to Phe and Try, respectively.[50]

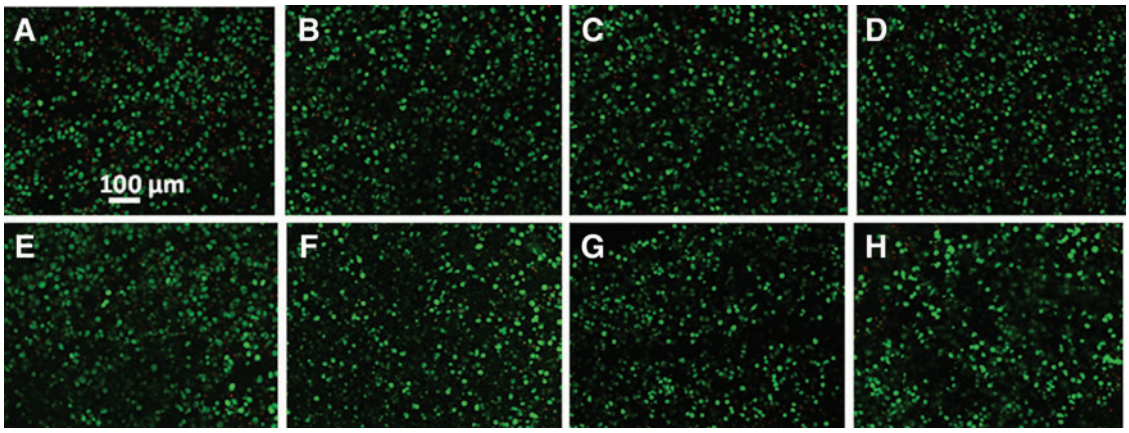


**FIG. 4.** Live/dead analysis of control and nanoceria-containing constructs on day 30. Green color indicates live cells and red color indicates dead cells. Constructs were cultured without IL-1α insult (top row) or with 10 ng/mL IL-1α from days 16 to 30 (bottom row). **(A, E)** Control (0 μg/mL of nanoceria), **(B, F)** 10 μg/mL, **(C, G)** 100 μg/mL, and **(D, H)** 1000 μg/mL of nanoceria. No discernable differences were observed between groups. Color images available online at www.liebertpub.com/tea

*Study 2*

In this study, engineered cartilage was cultured with CM supplemented with nanoceria particles. The rationale for adding nanoceria directly to the growth medium was to deactivate the effects of inflammation caused by the IL-1α insult at the outer layers of scaffold itself. The concentrations of nanoceria in suspension were 0, 100, and 1000 μg/mL, with the 0 μg/mL serving as the control.

A statistically significant downregulation of mechanical properties and GAG content was observed due to 0.5 ng/mL of IL-1α in control and experimental samples (Fig. 7). In the absence of IL-1α insult and in the presence of a low IL-1α concentration (0.5 ng/mL), constructs cultured with 1000 μg/mL nanoceria had the greatest mechanical properties ($n = 5$, $p < 0.05$ vs. control; Fig. 7). At a physiologically relevant concentration of IL-1α (0.5 ng/mL), nanoceria protected engineered cartilage from inflammatory damage at concentrations of 100 and 1000 μg/mL ($n = 5$, $p < 0.05$ vs. control). However, at the highest concentration of IL-1α (10 ng/mL), nanoceria did not protect the constructs against damage due to inflammation (Fig. 7).

## Discussion

Based on the findings of the studies reported here, we accept our hypothesis that nanoceria improves synthesis of ECM (GAGs). However, we conditionally accept the second hypothesis that nanoceria protects deposited ECM from IL-1α enzymatic insult.

Nanoceria particles (concentration range = 100–1000 μg/mL) embedded in the construct or delivered through the culture medium (both Study 1 and Study 2) improved tissue properties (Figs. 3 and 7). This effect was more pronounced for nanoceria-embedded constructs, where increases in biochemical contents corresponded to the improved dynamic and

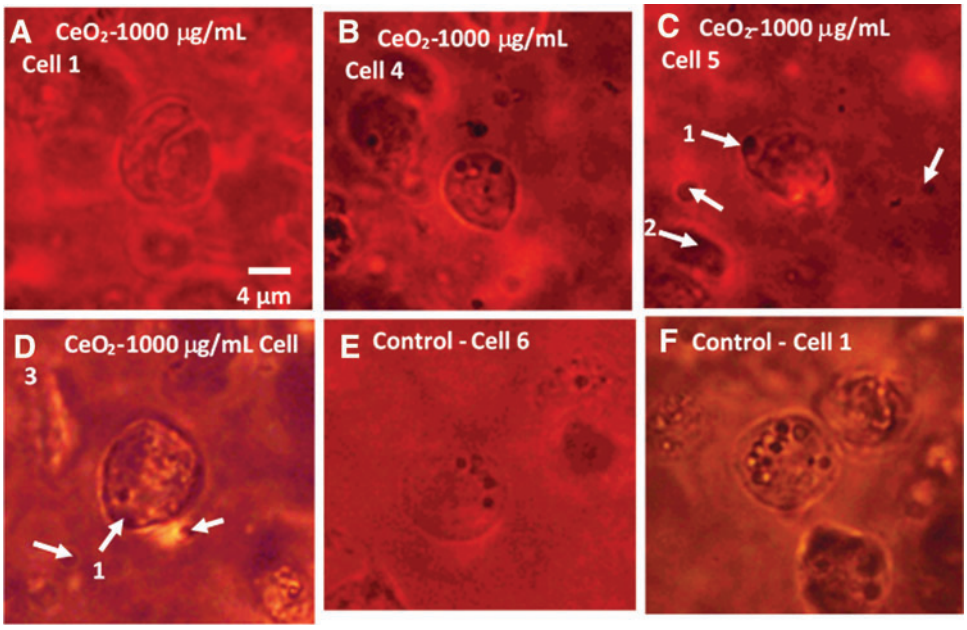


**FIG. 5.** Optical images of individual chondrocyte cells **(A–D)** cultured with 1000 μg/mL nanoceria and **(E, F)** two cells from a control sample (no nanoceria). Arrows 1 in **(C)** and **(D)** mark dark spots that are assumed to be nanoceria clusters on the basis of the absence of such spots in the samples not loaded with nanoparticles as well as on the basis of the Raman spectrum of the spot marked by arrow 2. Scale is the same. Color images available online at www.liebertpub.com/tea

Table 1. Diagnostic Peaks in Raman Spectra of Chondrocytes Used for the Analysis of Biochemical Changes

| *Raman shift, $cm^{-1}$* | *Biochemical characteristic* | *References* |
|---|---|---|
| 1004 | Symmetric ring breathing of phenylalanine<br>Absolute intensity of this peak is proportional to total protein in cells<br>Collagen backbone C−C stretching | 77,78<br>52,63,78,79 |
| 854, 925 | Pro | 80 |
| 940 | C−C stretching mode of α-helical structure of collagen | 61 |
| 960–970 | Nonhelical telopeptide/less-ordered collagen | This work on the basis of Refs. 81,82 |
| 480 | Endocyclic (CCO, CCC) deformations; glycogen content | 83–86 |
| 1043–1050 | C−OH stretching mode of pyranose ring; polysaccharide content | 81,83 |
| 1300 | $CH_2$ twisting mode of hydrocarbon chains; total lipids | 87 |
| 1657 | C=C stretching mode of unsaturated lipids (superimposed on the amide I peak of protein); total unsaturated lipids | 88 |
| ~1750 | C=O stretching mode of ester groups of lipids | 88 |
| ~790 | P−O stretching mode of phosphodiester ($C_5$-O-P-O-$C_3$) groups of DNA polysaccharide backbone structures; Total DNA | 77 |

Young's moduli, respectively (Fig. 3). We also suggest that nanoceria's radical-scavenging activity may be responsible for the improved biochemical and mechanical properties. These results for different mode of addition of nanoceria imply that in the absence of an external stress, the local redox environment near the chondrocytes controls the tissue growth and its properties *in vitro*. Therefore, the anabolic effects of nanoceria particles are better when embedded within the construct. Recently, beneficial effects of nanoceria for tissue engineering applications[35] and for accelerated wound healing[11] have been reported. Even though the increased scavenging of oxidant intermediates can be attributed to the increased accumulation of collagen, there is no direct evidence to substantiate it. Further, it has been observed that the dissolved cerium can enhance incorporation of proline in both collagen and non-collagen proteins.[36]

In this study, we evaluated the ability of nanoceria to combat the inflammatory action of IL-1α, specifically, the matrix degradation effects. In cartilage, IL-1α insult causes matrix degradation that inhibits intracellular biochemical synthesis.[51] The matrix degradation process stimulated by IL-1α is caused by the release of metalloproteinases and a decrease in extracellular pH, due to an increase in proton extrusion from chondrocytes to the extracellular environment.[52–54] Insignificant difference in

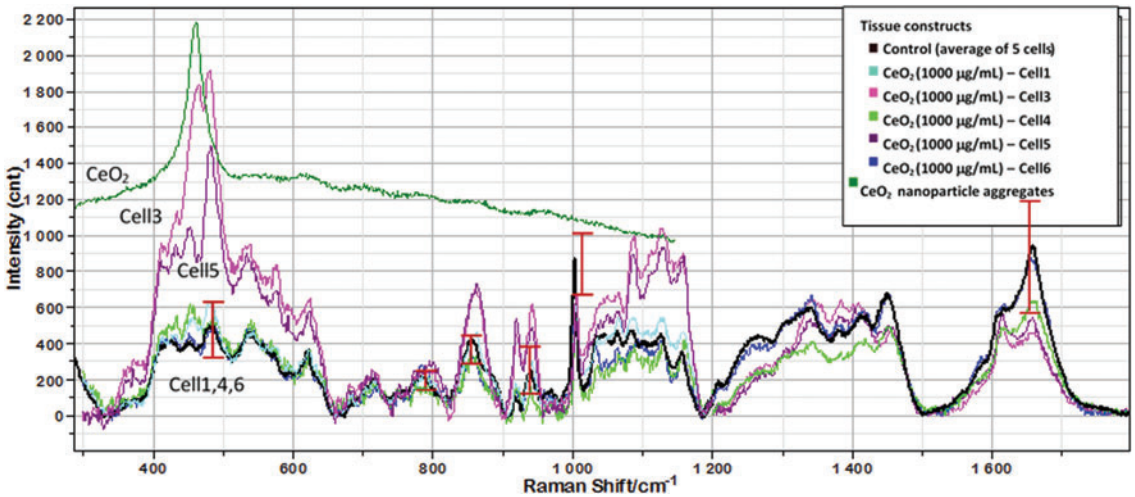


**FIG. 6.** Raman spectra of five individual chondrocytes (Nos. 1, 3–6) in a scaffold embedded with 1000 µg/mL nanoceria acquired at day 33 in comparison with an average spectrum of five control cells. For comparison, Raman spectrum of a nanoceria cluster in the scaffold is shown. Vertical bars show standard deviations in the main diagnostic peaks (Table 1) for the average spectrum of the control sample. The averaging procedure is shown in the Supplementary Data. Optical images of cells (No. 1, 3–5) are shown in Figure 5. Color images available online at www.liebertpub.com/tea

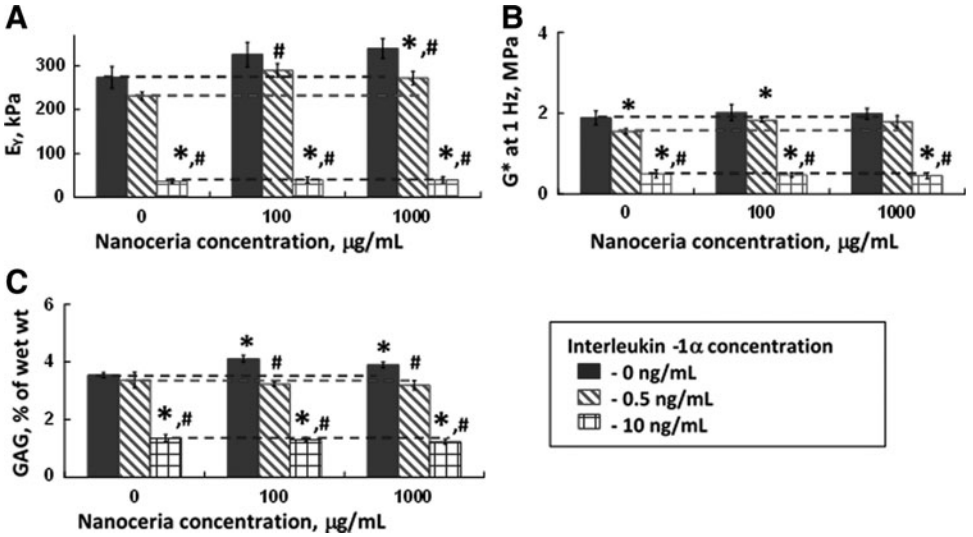


**FIG. 7.** Mechanical and biochemical properties of constructs from Study 2, where the growth medium was supplemented with nanoceria. **(A)** Equilibrium Young's modulus ($E_Y$), **(B)** dynamic modulus ($G^*$) at 1 Hz, and **(C)** GAG normalized by wet weight. IL-1α was added from day 21 to 34 and its concentrations are shown on the figure (0, 0.5, and 10 ng/mL). Dotted lines represent the control and are guidelines for comparison ($n = 4$–7 per group). Significant differences ($p \leq 0.05$) with respect to nanoceria concentration are noted by an asterisk (* vs. 0 μg/mL nanoceria). Differences with respect to IL-1α treatment are noted by # (vs. 0 ng/mL IL-1α). A statistically significant downregulation of mechanical properties and GAG content was observed due to 0.5 ng/mL IL-1α in control and experimental samples.

the DNA content (Fig. 3E) and live/dead analysis (Fig. 4) also suggest that of IL-1α, even at very high concentration, does not decrease chondrocyte viability but rather degrades the deposited ECM. In Study 2, where nanoceria is suspended in growth medium, 100 and 1000 μg/mL nanoceria groups partially prevented matrix degradation of engineered constructs exposed to physiological levels of IL-1α (0.5 ng/mL).[37,38] Delivery of nanoceria particles within the construct or through the culture medium did not protect the engineered cartilage from high concentrations of IL-1α (10 ng/mL). However, it should be noted that while the concentration of IL-1α used here (10 ng/mL) is typical of *in vitro* studies,[6,7,39,40] it is two orders of magnitude greater than the measured *in vivo* concentrations of IL-1α and IL-1β for arthritic or arthritic-like conditions.[37,38] Based on our findings, we conditionally accept our hypothesis that the detrimental effects of IL-1α can be deactivated by interacting with nanoceria and is comparable with observations by previous studies that have used mammalian cell lines.[10,15–18,55–57] However, further studies are necessary to determine the mechanism as well as effectiveness of nanoceria in deactivating IL-1α in chondrocytes in physiologically relevant conditions.

Raman microspectroscopy was used to verify the macroscopic data and to extract additional molecular-level information about the chondrocyte response to nanoceria. Previous studies have shown that vibrational spectroscopy method used in this study is versatile in its ability to noninvasively characterize the physiological status of individual cells at the molecular level.[58] Specifically, it has been used to monitor the impact of external stimuli and pathology on the content of proteins, membrane and nonmembrane lipids, DNA, and GAG, order of lipids, secondary and ternary structure of proteins, integrity of DNA, and redox state of cytochrome c. As compared with the conventional fluorescence-based assays, the Raman-based analysis does not use foreign molecular probes, which can affect the cells (e.g., Hoechst labeling of the nucleus).[59] Moreover, the spectroscopic nature of the method allows acquisition of a large body of the microscopic information from one spectrum of the cell acquired in a short time (30 min in our study). However, to the authors' best knowledge, this method has been applied to characterize individual chondrocytes only in one study, where molecular markers of the cell dedifferentiation in the 2D state were determined.[60]

Our study for the first time demonstrates the potential of Raman microspectroscopy in detecting *in vitro* molecular changes in individual chondrocytes embedded in agarose. In particular, the spectra suggest that there is a direct correlation between the intracellular and near-membrane presence of nanoceria and increased cellular synthesis of procollagen and glycogen, as well as a better ordering of procollagen. Moreover, the spectra do not reveal apoptotic changes, necrotic changes, or genotoxic effects due to nanoceria. This result agrees with the nanoceria-induced increase in the expression of the neuroprotection-associated genes and inhibition of the apoptosis signaling pathways, including downregulation of caspase-3.[55]

We rule out that the possibility of membrane protection by nanoceria against IL-1α as a reason for antioxidant effects since no visual aggregation of nanoceria outside of cell membrane was observed in the optical images. Thus, it is likely that the improved tissue properties and anti-inflammatory properties are due to intracellular effects.

At the same time, there are studies that reported adverse genomic and pro-oxidant cytotoxic effects due to nanoceria at different concentrations.[24–28,61–70] Specifically, nanoceria has been reported to be toxic to microbial and algal cells, which is correlated with the nanoparticle adsorption on the cell membrane.[64–66,68] It can also be toxic to mammalian cells, although the nanotoxicity mechanism appears to be different, including a rapid intracellular uptake[15,71,72] and

pro-oxidant effects.[73] The aspect ratio of nanoceria is a critical factor in determining its pro-oxidative effects.[29] Nanorods shorter than $\sim 200$ nm with an aspect ratio of $< 16$ were found to have little-to-no toxicity, which was attributed to the higher tendency of these nanorods to form bundles. However, their low toxicity may be due to the nanosize-induced increase in the $Ce^{3+}/Ce^{4+}$ ratio rather than their morphology. Although the molecular mechanisms of both the promoting and adverse effects of nanoceria are unclear at the moment, it can be speculated, on the basis of the high amount of $Ce^{3+}$ in the surface layer of the nanoparticles used in this study, that the antioxidant effects are related to the $Ce^{3+}/Ce^{4+}$ ratio since it determines the redox buffer and oxygen storage capacity of the nanoparticles. A further study using $CeO_2$ nanoparticles with different concentrations of $Ce^{3+}$ could clarify this important issue.

In conclusion, nanoceria particles at concentrations up to 1000 μg/mL were biocompatible with chondrocytes and improved mechanical and biochemical properties of engineered cartilage when embedded in the agarose scaffold. Further, the presence of nanoceria in the culture media partially protected the ECM from the inflammatory damage caused by physiological levels of IL-1α (0.5 ng/mL). Finally, our findings suggest that incorporation of nanoceria into a biological repair strategy may serve as a means of augmenting the engineered cartilage properties *in vitro* prior to implantation.

## Key Points

The effects of nanoceria on the *in vitro* culture of chondrocytes in agarose scaffolds and against the ECM degradation by exogenously added IL-1α were studied. It was found that

(1) At least up to a concentration of 1000 μg/mL, nanoceria is biocompatible toward chondrocytes (60,000 cells/μg of nanoceria).
(2) Nanoceria particles embedded within engineered cartilage constructs have a beneficial impact on the biochemical as well as mechanical properties of the cartilage tissue grown *in vitro*.
(3) The presence of nanoceria in the growth media partially protected the ECM from the inflammatory damage due to IL-1α (at a physiologically relevant concentration of 0.5 ng/mL). However, when IL-1α was present at very high concentration (10 ng/mL), no anti-inflammatory effect due to nanoceria was observed.
(4) For the first time, Raman microspectroscopy was applied *in vitro* to directly detect molecular changes in individual chondrocytes in 3D agarose scaffolds in response to a stimulus.
(5) The Raman analysis revealed that the presence of nanoceria near the cell membrane or inside the cells stimulates intercellular synthesis of procollagen and glycogen, and does not trigger apoptosis or necrosis of the cells.

## Acknowledgments

This material is based upon work partially supported by NIH grant AR46568, NSF under grant 0749461, as well as by NSF and the Environmental Protection Agency under Cooperative Agreement EF 0830117. The authors acknowledge partial support from Center for Particular and Surfactant Systems (CPaSS) at Columbia University and from the Tata Research Development and Design Center, Pune, India. We also thank Dr. X. Fang for the TEM image. We also thank Andrea Tan for her suggestions on interleukin insults on cartilage.

## Disclosure Statement

Authors hereby declare that there are no competing financial interests with respect to the reported results in this article.

## References

1. Rotter, N., Ung, F., Roy, A.K., Vacanti, M., Eavey, R.D., Vacanti, C.A., and Bonassar, L.J. Role for interleukin 1 alpha in the inhibition of chondrogenesis in autologous implants using polyglycolic acid-polylactic acid scaffolds. Tissue Eng **11,** 192, 2005.
2. Hung, C.T., Mauck, R.L., Wang, C.C.B., Lima, E.G., and Ateshian, G.A. A paradigm for functional tissue engineering of articular cartilage via applied physiologic deformational loading. Ann Biomed Eng **32,** 35, 2004.
3. Capito, R.M., and Spector, M. Scaffold-based articular cartilage repair. IEEE Eng Med Biol Mag **22,** 42, 2003.
4. Habibovic, P., Woodfield, T., de Groot, K., and van Blitterswijk, C. Predictive value of *in vitro* and *in vivo* assays in bone and cartilage repair: what do they really tell us about the clinical performance? In: Fisher J.P., ed. Tissue Engineering. Berlin: Springer-Verlag Berlin, 2006, p. 327.
5. Francioli, S., Cavallo, C., Grigolo, B., Martin, I., and Barbero, A. Engineered cartilage maturation regulates cytokine production and interleukin-1 beta response. Clin Orthop Relat Res **469,** 2773, 2011.
6. Lima, E.G., Tan, A.R., Tai, T., Bian, L., Stoker, A.M., Ateshian, G.A., Cook, J.L., and Hung, C.T. Differences in interleukin-1 response between engineered and native cartilage. Tissue Eng Part A **14,** 1721, 2008.
7. Lima, E.G., Tan, A.R., Tai, T., Marra, K.G., DeFail, A., Ateshian, G.A., and Hung, C.T. Genipin enhances the mechanical properties of tissue-engineered cartilage and protects against inflammatory degradation when used as a medium supplement. J Biomed Mater Res A **91A**, 692, 2009.
8. Tyler, J.A. Insulin-like growth factor-1 can decrease degradation and promote synthesis of proteoglycan in cartilage exposed to cytokines. Biochem J **260,** 543, 1989.
9. Hirst, S.M., Karakoti, A.S., Tyler, R.D., Sriranganathan, N., Seal, S., and Reilly, C.M. Anti-inflammatory properties of cerium oxide nanoparticles. Small **5,** 2848, 2009.
10. Niu, J.L., Azfer, A., Rogers, L.M., Wang, X.H., and Kolattukudy, P.E. Cardioprotective effects of cerium oxide nanoparticles in a transgenic murine model of cardiomyopathy. Cardiovasc Res **73,** 549, 2007.
11. Chigurupati, S., Mughal, M.R., Okun, E., Das, S., Kumar, A., McCaffery, M., Seal, S., and Mattson, M.P. Effects of cerium oxide nanoparticles on the growth of keratinocytes, fibroblasts and vascular endothelial cells in cutaneous wound healing. Biomaterials **34,** 2194, 2013.
12. Shiraishi, T., DeMeester, S.R., Worrall, N.K., Ritter, J.H., Misko, T.P., Ferguson, Jr., T.B., Cooper, J.D., and Patterson, G.A. Inhibition of inducible nitric oxide synthase

ameliorates rat lung allograft rejection. J Thorac Cardiovasc Surg **110,** 1449, 1995.
13. McDermott, C.D., Gavita, S.M., Shennib, H., and Giaid, A. Immunohistochemical localization of nitric oxide synthase and the oxidant peroxynitrite in lung transplant recipients with obliterative bronchiolitis. Transplantation **64,** 270, 1997.
14. Das, M., Patil, S., Bhargava, N., Kang, J.F., Riedel, L.M., Seal, S., and Hickman, J.J. Auto-catalytic ceria nanoparticles offer neuroprotection to adult rat spinal cord neurons. Biomaterials **28,** 1918, 2007.
15. Schubert, D., Dargusch, R., Raitano, J., and Chan, S.W. Cerium and yttrium oxide nanoparticles are neuroprotective. Biochem Biophys Res Commun **342,** 86, 2006.
16. Chen, J.P., Patil, S., Seal, S., and McGinnis, J.F. Rare earth nanoparticles prevent retinal degeneration induced by intracellular peroxides. Nat Nanotechnol **1,** 142, 2006.
17. Amin, K.A., Hassan, M.S., Awad, E.T., and Hashem, K.S. The protective effects of cerium oxide nanoparticles against hepatic oxidative damage induced by monocrotaline. Int J Nanomed **6,** 143, 2011.
18. Clark, A., Zhu, A.P., Sun, K., and Petty, H.R. Cerium oxide and platinum nanoparticles protect cells from oxidant-mediated apoptosis. J Nanopart Res **13,** 5547, 2011.
19. Horie, M., Nishio, K., Kato, H., Fujita, K., Endoh, S., Nakamura, A., Miyauchi, A., Kinugasa, S., Yamamoto, K., Niki, E., Yoshida, Y., Hagihara, Y., and Iwahashi, H. Cellular responses induced by cerium oxide nanoparticles: induction of intracellular calcium level and oxidative stress on culture cells. J Biochem **150,** 461, 2011.
20. Alili, L., Sack, M., Karakoti, A.S., Teuber, S., Puschmann, K., Hirst, S.M., Reilly, C.M., Zanger, K., Stahl, W., Das, S., Seal, S., and Brenneisen, P. Combined cytotoxic and anti-invasive properties of redox-active nanoparticles in tumor-stroma interactions. Biomaterials **32,** 2918, 2011.
21. Tarnuzzer, R.W., Colon, J., Patil, S., and Seal, S. Vacancy engineered ceria nanostructures for protection from radiation-induced cellular damage. Nano Lett **5,** 2573, 2005.
22. Colon, J., Hsieh, N., Ferguson, A., Kupelian, P., Seal, S., Jenkins, D.W., and Baker, C.H. Cerium oxide nanoparticles protect gastrointestinal epithelium from radiation-induced damage by reduction of reactive oxygen species and upregulation of superoxide dismutase 2. Nanomedicine **6,** 698, 2010.
23. Babu, S., Cho, J.H., Dowding, J.M., Heckert, E., Komanski, C., Das, S., Colon, J., Baker, C.H., Bass, M., Self, W.T., and Seal, S. Multicolored redox active upconverter cerium oxide nanoparticle for bio-imaging and therapeutics. Chem Commun **46,** 6915, 2010.
24. Lin, W.S., Huang, Y.W., Zhou, X.D., and Ma, Y.F. Toxicity of cerium oxide nanoparticles in human lung cancer cells. Int J Toxicol **25,** 451, 2006.
25. Srinivas, A., Rao, P.J., Selvam, G., Murthy, P.B., and Reddy, P.N. Acute inhalation toxicity of cerium oxide nanoparticles in rats. Toxicol Lett **205,** 105, 2011.
26. Park, E.J., Choi, J., Park, Y.K., and Park, K. Oxidative stress induced by cerium oxide nanoparticles in cultured BEAS-2B cells. Toxicology **245,** 90, 2008.
27. Nalabotu, S.K., Kolli, M.B., Triest, W.E., Ma, J.Y., Manne, N., Katta, A., Addagarla, H.S., Rice, K.M., and Blough, E.R. Intratracheal instillation of cerium oxide nanoparticles induces hepatic toxicity in male Sprague-Dawley rats. Int J Nanomed **6,** 2327, 2011.
28. Cho, W.S., Duffin, R., Poland, C.A., Howie, S.E.M., MacNee, W., Bradley, M., Megson, I.L., and Donaldson, K. Metal oxide nanoparticles induce unique inflammatory footprints in the lung: important implications for nanoparticle testing. Environ Health Perspect **118,** 1699, 2010.
29. Ji, Z., Wang, X., Zhang, H., Lin, S., Meng, H., Sun, B., George, S., Xia, T., Nel, A.E., and Zink, J.I. Designed synthesis of $CeO_2$ nanorods and nanowires for studying toxicological effects of high aspect ratio nanomaterials. ACS Nano **6**, 5366, 2012.
30. Karakoti, A.S., Munusamy, P., Hostetler, K., Kodali, V., Kuchibhatla, S., Orr, G., Pounds, J.G., Teeguarden, J.G., Thrall, B.D., and Baer, D.R. Preparation and characterization challenges to understanding environmental and biological impacts of ceria nanoparticles. Surf Interface Anal **44,** 882, 2012.
31. Celardo, I., Pedersen, J.Z., Traversa, E., and Ghibelli, L. Pharmacological potential of cerium oxide nanoparticles. Nanoscale **3,** 1411, 2011.
32. Karakoti, A., Singh, S., Dowding, J.M., Seal, S., and Self, W.T. Redox-active radical scavenging nanomaterials. Chem Soc Rev **39,** 4422, 2010.
33. Karakoti, A.S., Singh, S., Kumar, A., Malinska, M., Kuchibhatla, S.V.N.T., Wozniak, K., Self, W.T., and Seal, S. PEGylated nanoceria as radical scavenger with tunable redox chemistry. J Am Chem Soc **131,** 14144, 2009.
34. Benton, H.P., and Tyler, J.A. Inhibition of cartilage proteoglycan synthesis by interleukin-1. Biochem Biophys Res Commun **154,** 421, 1988.
35. Karakoti, A.S., Tsigkou, O., Yue, S., Lee, P.D., Stevens, M.M., Jones, J.R., and Seal, S. Rare earth oxides as nanoadditives in 3-D nanocomposite scaffolds for bone regeneration. J Mat Chem **20,** 8912, 2010.
36. Shivakumar, K., Nair, R.R., and Valiathan, M.S. Paradoxical effect of cerium on collagen-synthesis in cardiac fibroblasts. J Mol Cell Cardiol **24,** 775, 1992.
37. Kahle, P., Saal, J.G., Schaudt, K., Zacher, J., Fritz, P., and Pawelec, G. Determination of cytokines in synovial fluids: correlation with diagnosis and histomorphological characteristics of synovial tissue. Ann Rheum Dis **51,** 731, 1992.
38. Vaatainen, U., Lohmander, L.S., Thonar, E., Hongisto, T., Agren, U., Ronkko, S., Jaroma, H., Kosma, V.M., Tammi, M., and Kiviranta, I. Markers of cartilage and synovial metabolism in joint fluid and serum of patients with chondromalacia of the patella. Osteoarthritis Cartilage **6,** 115, 1998.
39. Ismaiel, S., Atkins, R.M., Pearse, M.F., Dieppe, P.A., and Elson, C.J. Susceptibility of normal and arthritic human articular cartilage to degradative stimuli. Br J Rheumatol **31,** 369, 1992.
40. Lima, E.G., Tan, A.R., Tai, T., Bian, L., Ateshian, G.A., Cook, J.L., and Hung, C.T. Physiologic deformational loading does not counteract the catabolic effects of interleukin-1 in long-term culture of chondrocyte-seeded agarose constructs. J Biomech **41,** 3253, 2008.
41. Mauck, R.L., Soltz, M.A., Wang, C.C.-B., Wong, D.D., Chao, P.-H.G., Valhmu, W.B., Hung, C.T., and Ateshian, G.A. Functional tissue engineering of articular cartilage through dynamic loading of chondrocyte-seeded agarose gels. J Biomech Eng **122,** 252, 2000.

42. Kelly, T.A.N., Ng, K.W., Wang, C.C.B., Ateshian, G.A., and Hung, C.T. Spatial and temporal development of chondrocyte-seeded agarose constructs in free-swelling and dynamically loaded cultures. J Biomech **39,** 1489, 2006.
43. Farndale, R.W., Buttle, D.J., and Barrett, A.J. Improved quantitation and discrimination of sulfated glycosaminoglycans by use of dimethylmethylene blue. Biochim Biophys Acta **883,** 173, 1986.
44. Farndale, R.W., Sayers, C.A., and Barrett, A.J. A direct spectrophotometric micro-assay for sulfated glycosaminoglycans in cartilage cultures. Connect Tissue Res **9,** 247, 1982.
45. Stegeman, H., and Stalder, K. Determination of hydroxyproline. Clin Chim Acta **18,** 267, 1967.
46. Ong, Y.H., Lim, M., and Liu, Q. Comparison of principal component analysis and biochemical component analysis in Raman spectroscopy for the discrimination of apoptosis and necrosis in K562 leukemia cells. Opt Express **20,** 25041, 2012.
47. Bonifacio, A., Beleites, C., Vittur, F., Marsich, E., Semeraro, S., Paoletti, S., and Sergo, V. Chemical imaging of articular cartilage sections with Raman mapping, employing uni- and multi-variate methods for data analysis. Analyst **135,** 3193, 2010.
48. De Gelder, J., De Gussem, K., Vandenabeele, P., and Moens, L. Reference database of Raman spectra of biological molecules. J Raman Spectrosc **38,** 1133, 2007.
49. Zoladek, A., Pascut, F.C., Patel, P., and Notingher, I. Noninvasive time-course imaging of apoptotic cells by confocal Raman micro-spectroscopy. J Raman Spectrosc **42,** 251, 2011.
50. El-Said, W.A., Kim, T.H., Kim, H., and Choi, J.W. Analysis of intracellular state based on controlled 3D nanostructures mediated surface enhanced Raman scattering. PLoS One **6,** e15836, 2011.
51. Neidel, J., and Zeidler, U. Independent effects of interleukin 1 on proteoglycan synthesis and proteoglycan breakdown of bovine articular cartilage *in vitro*. Agents Actions **39,** 82, 1993.
52. Yocum, S.A., Lopresti-Morrow, L.L., Gabel, C.A., Milici, A.J., and Mitchell, P.G. Bafilomycin A1 inhibits IL-1-stimulated proteoglycan degradation by chondrocytes without affecting stromelysin synthesis. Arch Biochem Biophys **316,** 827, 1995.
53. Tattersall, A.L., Browning, J.A., and Wilkins, R.J. Modulation of H+ transport mechanisms by interleukin-1 in isolated bovine articular chondrocytes. Cell Physiol Biochem **16,** 43, 2005.
54. Flannery, C.R., Little, C.B., Caterson, B., and Hughes, C.E. Effects of culture conditions and exposure to catabolic stimulators (IL-1 and retinoic acid) on the expression of matrix metalloproteinases (MMPs) and disintegrin metalloproteinases (ADAMs) by articular cartilage chondrocytes. Matrix Biol **18,** 225, 1999.
55. Kong, L., Cai, X., Zhou, X.H., Wong, L.L., Karakoti, A.S., Seal, S., and McGinnis, J.F. Nanoceria extend photoreceptor cell lifespan in tubby mice by modulation of apoptosis/survival signaling pathways. Neurobiol Dis **42,** 514, 2011.
56. Pierscionek, B.K., Li, Y.B., Yasseen, A.A., Colhoun, L.M., Schachar, R.A., and Chen, W. Nanoceria have no genotoxic effect on human lens epithelial cells. Nanotechnology **21,** 035102, 2010.
57. Cai, X., Sezate, S.A., and McGinnis, J.F. Neovascularization: ocular diseases, animal models and therapies. In: LaVail M.M., Ash J.D., Anderson R.E., Hollyfield J.G., and Grimm C., eds. Retinal Degenerative Diseases. Berlin: Springer-Verlag Berlin, 2012, p. 245.
58. Notingher, I., and Hench, L.L. Raman microspectroscopy: a noninvasive tool for studies of individual living cells *in vitro*. Expert Rev Med Devices **3,** 215, 2006.
59. Fore, S., Chan, J., Taylor, D., and Huser, T. Raman spectroscopy of individual monocytes reveals that single-beam optical trapping of mononuclear cells occurs by their nucleus. J Opt **13,** 044021, 2011.
60. Pudlas, M., Brauchle, E., Klein, T.J., Hutmacher, D.W., and Schenke-Layland, K. Non-invasive identification of proteoglycans and chondrocyte differentiation state by Raman microspectroscopy. J Biophotonics **6,** 205, 2013.
61. Lee, S.S., Zhu, H.G., Contreras, E.Q., Prakash, A., Puppala, H.L., and Colvin, V.L. High temperature decomposition of cerium precursors to form ceria nanocrystal libraries for biological applications. Chem Mater **24,** 424, 2012.
62. García, A., Delgado, L., Torà, J.A., Casals, E., González, E., Puntes, V., Font, X., Carrera, J., and Sánchez, A. Effect of cerium dioxide, titanium dioxide, silver, and gold nanoparticles on the activity of microbial communities intended in wastewater treatment. J Hazard Mater **199–200,** 64, 2012.
63. García, A., Espinosa, R., Delgado, L., Casals, E., González, E., Puntes, V., Barata, C., Font, X., and Sánchez, A. Acute toxicity of cerium oxide, titanium oxide and iron oxide nanoparticles using standardized tests. Desalination **269,** 136, 2011.
64. Rodea-Palomares, I., Boltes, K., Fernandez-Pinas, F., Leganes, F., Garcia-Calvo, E., Santiago, J., and Rosal, R. Physicochemical characterization and ecotoxicological assessment of CeO(2) nanoparticles using two aquatic microorganisms. Toxicol Sci **119,** 135, 2011.
65. Thill, A., Zeyons, O., Spalla, O., Chauvat, F., Rose, J., Auffan, M., and Flank, A.M. Cytotoxicity of $CeO_2$ nanoparticles for *Escherichia coli*. Physico-chemical insight of the cytotoxicity mechanism. Environ Sci Technol **40,** 6151, 2006.
66. Rogers, N.J., Franklin, N.M., Apte, S.C., Batley, G.E., Angel, B.M., Lead, J.R., and Baalousha, M. Physicochemical behaviour and algal toxicity of nanoparticulate CeO(2) in freshwater. Environ Chem **7,** 50, 2010.
67. Van Hoecke, K., Quik, J.T.K., Mankiewicz-Boczek, J., De Schamphelaere, K.A.C., Elsaesser, A., Van der Meeren, P., Barnes, C., McKerr, G., Howard, C.V., Van De Meent, D., Rydzynski, K., Dawson, K.A., Salvati, A., Lesniak, A., Lynch, I., Silversmit, G., De Samber, B., Vincze, L., and Janssen, C.R. Fate and Effects of CeO(2) Nanoparticles in aquatic ecotoxicity tests. Environ Sci Technol **43,** 4537, 2009.
68. Pelletier, D.A., Suresh, A.K., Holton, G.A., McKeown, C.K., Wang, W., Gu, B.H., Mortensen, N.P., Allison, D.P., Joy, D.C., Allison, M.R., Brown, S.D., Phelps, T.J., and Doktycz, M.J. Effects of engineered cerium oxide nanoparticles on bacterial growth and viability. Appl Environ Microbiol **76,** 7981, 2010.
69. Auffan, M., Rose, J., Orsiere, T., De Meo, M., Thill, A., Zeyons, O., Proux, O., Masion, A., Chaurand, P., Spalla,

O., Botta, A., Wiesner, M.R., and Bottero, J.Y. CeO(2) nanoparticles induce DNA damage towards human dermal fibroblasts *in vitro*. Nanotoxicology **3,** 161, 2009.

70. Lee, T.-L., Raitano, J.M., Rennert, O.M., Chan, S.-W., and Chan, W.-Y. Accessing the genomic effects of naked nanoceria in murine neuronal cells. Nanomedicine **8,** 599, 2012.
71. Singh, S., Kumar, A., Karakoti, A., Seal, S., and Self, W.T. Unveiling the mechanism of uptake and sub-cellular distribution of cerium oxide nanoparticles. Mol Biosyst **6,** 1813, 2010.
72. Raemy, D.O., Limbach, L.K., Rothen-Rutishauser, B., Grass, R.N., Gehr, P., Birbaum, K., Brandenberger, C., Gunther, D., and Stark, W.J. Cerium oxide nanoparticle uptake kinetics from the gas-phase into lung cells *in vitro* is transport limited. Eur J Pharm Biopharm **77,** 368, 2011.
73. Eom, H.J., and Choi, J. Oxidative stress of CeO(2) nanoparticles via p38-Nrf-2 signaling pathway in human bronchial epithelial cell, Beas-2B. Toxicol Lett **187,** 77, 2009.

Address correspondence to:
*Ponisseril Somasundaran, PhD*
*Department of Earth and Environmental Engineering*
*Columbia University*
*500 W, 120th Street*
*Mudd 918*
*New York, NY 10027*

*E-mail:* ps24@columbia.edu

*Received: September 20, 2013*
*Accepted: April 24, 2014*
*Online Publication Date: June 23, 2014*